# A theoretical study of the $^1B_{2u}$ and $^1B_{1u}$ vibronic bands in benzene

Anders Bernhardsson, Niclas Forsberg, Per-Åke Malmqvist, and Björn O. Roos
*Department of Theoretical Chemistry, Chemical Center, University of Lund, P.O. Box 124,*
*S-221 00 Lund, Sweden*

Luis Serrano-Andrés
*Departamento de Química Física, Universitat de València, Dr. Moliner 50, Burjassot,*
*E-46100 Valencia, Spain*

The two lowest bands, $^1B_{2u}$ and $^1B_{1u}$, of the electronic spectrum of the benzene molecule have been studied theoretically using a new method to compute vibronic excitation energies and intensities. The complete active space (CAS) self-contained field (SCF) method (with six active $\pi$-orbitals) was used to compute harmonic force field for the ground state and the $^1B_{2u}$ and $^1B_{1u}$ electronic states. A linear approximation has been used for the transition dipole as a function of the nuclear displacement coordinates. Derivatives of the transition dipole were computed using a variant of the CASSCF state interaction method. Multiconfigurational second-order perturbation theory (CASPT2) was used to obtain absolute excitation energies (12 active $\pi$-orbitals). The results show that the approach works well. Vibrational progressions are well described in both bands and intensities, and energies are in agreement with experiment, in particular when CASPT2 derived geometries are used. One interesting result is that computed vertical energies fall about 0.1 eV on the high energy side of the band maximum. © *2000 American Institute of Physics.*
[S0021-9606(00)30306-3]

## I. INTRODUCTION

Vibronic spectra can be predicted by quantum chemical methods provided proper force fields and electronic transition strengths are available. Accurate vibrational spectra for ground states can often be obtained by comparably cheap methods such as Møller–Plesset second-order perturbation theory (MP2). Correction procedures, such as scaling, have been designed to account for remaining inaccuracies in the quantum chemical treatment, anharmonic effects, vibronic and Coriolis coupling, etc. For excited states, the situation is different.

For small systems, the best routinely available methods for potential surface calculations are the coupled-cluster method with triples correction [CCSD(T)] or for degenerate systems the multireference configuration interaction (MRCI) method with up to double external excitations. However, the computational cost of these methods is large and rises steeply with the size of the molecule, especially since large basis sets are required.[1] An account of the state of the art in *ab initio* calculations may be found in a recent review book edited by Langhoff.[2]

Here we shall demonstrate the usefulness of another approach, which may be applied to larger systems with less computational costs. This is the CASSCF (complete active space self-consistent field) method, followed by a perturbative estimate of the dynamic correlation energy (complete active space perturbation theory through second-order, CASPT2), which has emerged as a powerful method for the study of electronic excitations in organic molecules. However, derivatives are not yet available with this method.

In the present article, we therefore study the possibility to use the CASSCF method to compute geometries and force fields combined with CASPT2 correction for the total energies. Analytical second derivatives of CASSCF energies with respect to nuclear coordinates may easily be computed and in the present implementation also first derivatives of transition properties. It is then interesting to see how far such calculations can aid in the interpretation of electronic spectra. At the lowest level of ambition, a single-point calculation for each state gives immediately the so-called double harmonic approximation, if the transition moments are assumed to vary linearly with the displacement away from equilibrium.

Sometimes the coupling between different electronic states due to nonadiabatic coupling is of importance. We expect that incorporation of derivative coupling will first be done at this level of approximation, since the quantities—the derivative couplings—needed can be readily obtained by the same kind of approach as the derivatives of properties. The present article thus represents a first step in a line of development, which may later go beyond the adiabatic approximation.

Here, the $^1B_{2u} \leftarrow \tilde{X}$ and the $^1B_{1u} \leftarrow \tilde{X}$ transitions in benzene are studied. These are vertically forbidden, so all transition intensities will be due to Herzberg–Teller coupling, i.e., the first derivative of the transition dipole moment functions.

The electronic structure of benzene has been carefully studied (see for instance Refs. 3–5). Its valence-$\pi$ electronic structure is characterized by the highest occupied $(a_{2u})^2(e_{1g})^4$ and the lowest unoccupied $(e_{2u})^0(b_{2g})^0$ molecular orbitals. A single excitation $e_{1g} \rightarrow e_{2u}$ gives rise to three singlet states (experimental band maxima in parentheses):[6,7] $^1B_{2u}$ (4.90 eV), $^1B_{1u}$ (6.20 eV), and $^1E_{1u}$ (6.94 eV), the latter giving a one-photon symmetry allowed

J. Chem. Phys., Vol. 112, No. 6, 8 February 2000

$^1B_{2u}$ and $^1B_{1u}$ states of benzene    2799

transition to the ground state. Further valence $\pi \rightarrow \pi^*$ transitions are observed at higher energy, such as $^1E_{2g} \leftarrow \tilde{X}$ at about 7.8 eV.[8] Assignment of the bands in the electronic spectrum of benzene has been much discussed since the early experimental works.[3] Recent *ab initio* calculations[9–13] led to unambiguous assignments of the main vertical features (also Rydberg states), except perhaps for the $^1E_{2g}$ state, a multiconfigurational state which only the CASSCF/CASPT2 method[9,10] seems to treat properly.

Transitions from the ground state to the low-lying $^1B_{2u}$ and $^1B_{1u}$ excited states of benzene are (one-photon) symmetry forbidden. The transitions can be understood from either of two points of view. One way of reasoning is to regard the nuclear and electronic wave functions as completely decoupled, at zero-order. In this picture, the allowed vibronic transitions arise because the interaction between nuclear and electronic motion acts as a perturbation, causing a zero-order vibronic state with a pure $^1B_{2u}$ or $^1B_{1u}$ electronic wave function to mix with nearby vibronic states with the same combined symmetry, having an $^1E_{1u}$ electronic wave function. Thus it also acquires some nonzero transition dipole moment with the ground state. This ''intensity borrowing'' neatly explains some features, such that the intensity is larger when the borrowing band is close to the symmetry allowed band and that (if the borrowing is large) a corresponding decreased strength can be observed in the allowed transitions.

On the other hand, a nonzero value of certain symmetry coordinates will break the $D_{6h}$ symmetry of the electronic wave function, thus giving a nonzero transition dipole moment to the ground state. Multiplication with initial and final nuclear wave function can give a symmetric integrand and thus a nonzero dipole transition strength, if the upper state is also vibrationally excited. This is how the transition strengths are computed in this article. We have computed the electronic wave functions by the CASSCF method, obtaining analytically the second derivatives of the energy and first derivatives of the transition dipole moments at the equilibrium geometry.

A number of recent studies can be found in the literature, which describe forbidden transitions at the *ab initio* level.[14–17] However, in the present work a more elaborate and accurate description of the vibrational wave function and the geometry dependence of the transition dipole moment is used.

## II. METHODS

### A. The electronic structure

For a description of the complete active space (CAS) SCF method, see Ref. 18. For the present purpose, it is sufficient to note that this method accounts for all configuration mixing within a selected set of active orbitals, while lower-lying inactive orbitals are kept doubly occupied. The orbitals are optimized to minimize the energy. The valence $\pi$ orbitals were active and thus all configurations with six electrons distributed among these six $\pi$-orbitals are used, a space which suffices to compute the energy surfaces for the two lowest valence excited states at least close to their equilibrium geometries.[9]

The optimized geometries and analytical second derivatives of the energy with respect to the nuclear coordinates for the ground $1\,^1A_{1g}$ state and the excited $1\,^1B_{2u}$ and $1\,^1B_{1u}$ states were computed by a recently developed CASSCF linear response program.[19] Analytical first derivatives of the transition dipole moment for the transitions from the ground to the excited states have been computed at the same level. These derivatives were obtained by modifying the CAS state interaction method (CASSI),[20] which is normally used to compute matrix elements between CASSCF wave functions. By using the results from a multiconfigurational linear response calculation, the needed matrix elements involving *differentiated* wave functions are obtained. Averaged atomic natural orbital (ANO)-type basis sets[21] contracted to $[4s3p2d]$ for carbon and $[3s2p]$ for hydrogen have been used. Absolute excitation energies have been obtained with the CASPT2 method.[22–24] Somewhat larger ANO basis sets were used for these calculations: $[C/4s3p2d1f/H/3s2p1d]$.

### B. The vibrational wave function

The vibrational wave functions correspond to harmonic oscillators, with force fields taken directly from the second derivatives with no adjustment for anharmonicity.[25] The vibrational modes are numbered following Wilson's convention,[26] and when necessary, the number by Herzberg's convention[3] is also indicated.

The probability per unit time for a transition between two states is primarily determined by the square of the relevant transition matrix element.[27] For one-photon processes and within the electric dipole approximation, this is the transition dipole moment. Within the Born–Oppenheimer approximation, the vibronic wave function can be written as a product of a vibrational wave function ($\phi$) with an adiabatic electronic wave function ($\psi$):

$$\Psi_{v\alpha}(\mathbf{Q},\mathbf{q}) = \phi_{v\alpha}(\mathbf{Q})\psi_\alpha(\mathbf{Q},\mathbf{q}),$$

where $\mathbf{Q}$ are the nuclear and $\mathbf{q}$ the electronic coordinates. The vibrational wave function is the $v$th solution of the nuclear Schrödinger equation, using the adiabatic potential function for the electronic state $\alpha$.

The transition dipole moment matrix element is then given as

$$\mathbf{M}_{\alpha\beta}(v',v'') = \int \phi^*_{v'\alpha}(\mathbf{Q})\mu_{\alpha\beta}(\mathbf{Q})\phi_{v''\beta}(\mathbf{Q})\,d^N\mathbf{Q}, \qquad (1)$$

where $\mu_{\alpha\beta}(\mathbf{Q})$ is the electronic transition dipole moment. The dependence on orientation of the nuclear frame is ignored here i.e., *the rotation of the molecule is ignored*.

Expanding the electronic transition moment as a Taylor series in the nuclear coordinates about the equilibrium nuclear configuration, $\mathbf{Q}_0$, gives through first order

$$\mathbf{M}_{\alpha\beta}(v',v'') = \mu_{\alpha\beta}(\mathbf{Q}_0)\langle\phi_{v'\alpha}|\phi_{v''\beta}\rangle$$

$$+ \sum_i \left(\frac{\partial\mu_{\alpha\beta}}{\partial Q_i}\right)\langle\phi_{v'\alpha}|Q_i|\phi_{v''\beta}\rangle + \cdots. \quad (2)$$

The Condon approximation requires the neglect of all but the first term, which usually dominates for one-photon symmetry-allowed transitions. The other terms represent an

electronic transition moment induced by distortion away from the equilibrium. This is known as Herzberg–Teller vibronic coupling and the present approach will include first derivatives only, as shown in the formula above.

The transition moment function is considered to be linear in the chosen coordinates, and thus the matrix elements are easily expressed using harmonic oscillator ladder operators which create or annihilate a single quantum. The matrix elements are thus expressed in terms of Franck–Condon factors (i.e., overlaps between the two sets of harmonic oscillator functions involved in the transition), where a single vibrational quantum has been added to or removed from one of the states. In general, matrix elements of any polynomial in one or many coordinates over displaced harmonic oscillators with different force constants can be evaluated in terms of overlaps. A program for this kind of analysis, using a new method for evaluating the Franck–Condon factors[28] was used to evaluate the vibronic transition moment matrix elements.

If the electronic transition dipole moment was truly a linear function of the displacements, it could be evaluated anywhere. In order to minimize the inaccuracy inherent in the approximation, an average of its value in the two equilibria should be used, or it may be evaluated at an intermediate conformation. Here, the derivative of the wave function is evaluated at the intermediate expansion point, where the overlap between the vibrational wave functions from the two states are maximum.

The theoretical spectra computed in the present study were convoluted with a Lorentzian function of full width at half maximum,[15] $\Gamma = h/(4\pi T_2)$ corresponding to a fictitious lifetime $T_2 = 130$ fs for the $^1B_{2u}$ and $T_2 = 7$ fs for the $^1B_{1u}$ state, to account for the finite experimental resolution and for degrees of freedom not considered here, such as rotation. All calculations have been performed with the MOLCAS-4.1 (Ref. 29) program package.

### 1. Technical aspects of transition intensity calculations

We have used the LU method for calculating the Franck–Condon overlaps. What follows is a brief introduction to the basic concepts of the method and a few details about the implementation. For simplicity, the method is outlined for a one-dimensional case.

The vibrational wave functions for the ground state and for the excited state are taken to be harmonic oscillator functions. In addition to these two sets of wave functions, $\{\phi_k', \phi_k''\}$, we introduce an additional set of wave functions, $\{\phi_k\}$, such that[28]

$$\phi_0' = Ke^{\theta}\phi_0, \quad \phi_0'' = Ke^{-\theta}\phi_0. \tag{3}$$

Using ladder operators $\hat{a}$ and $\hat{b}$, an arbitrary overlap matrix element is

$$\langle \phi_m' | \phi_n'' \rangle = \frac{1}{m!n!} \langle (\hat{a}^\dagger)^m \phi_0' | (\hat{b}^\dagger)^n \phi_0'' \rangle$$

$$= \langle \phi_0' | \phi_0'' \rangle = \frac{1}{\sqrt{m!n!}} \langle (\phi_0)(\hat{X})^m (\hat{Y}^\dagger)^n | \phi_0 \rangle, \tag{4}$$
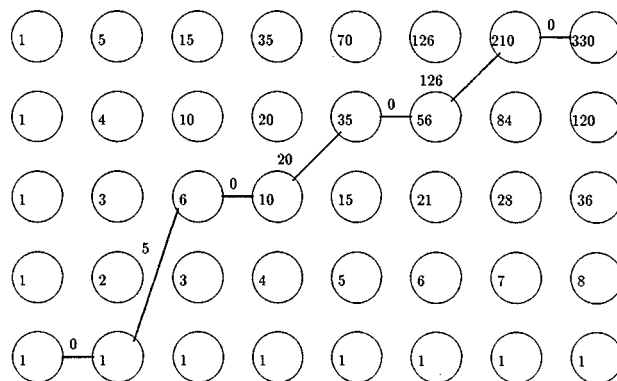


FIG. 1. A state path for four quanta distributed among eight oscillators with the quantum number string $1^0 2^0 3^2 4^0 5^1 6^0 7^1 8^0$.

where

$$\hat{X} = e^{\theta}(\hat{a})e^{-\theta} \quad \hat{Y} = e^{\theta}(\hat{b})e^{-\theta}. \tag{5}$$

Reexpressing $\hat{X}$ and $\hat{Y}$ using the step operators for the set $\{\phi_k\}$ allows us to obtain simple recursion formulas for

$$L_{mt} = \frac{1}{\sqrt{m!}} \langle \phi_0 | \hat{X}^m \phi_t \rangle, \tag{6}$$

$$U_{tn} = \frac{1}{\sqrt{n!}} \langle \phi_0 | \hat{Y}^n \phi_t \rangle. \tag{7}$$

After inserting a resolution of the identity in Eq. (4), we end up with the following formula for the overlaps:

$$\langle \phi_m' | \phi_n'' \rangle = \langle \phi_0' | \phi_0'' \rangle \sum_{t=0}^{\min(m,n)} L_{mt} U_{tn}. \tag{8}$$

Also, the matrix elements of any general operator $\hat{F}$ can be calculated,

$$\langle \phi_m' | \hat{F} | \phi_n'' \rangle = \langle \phi_0' | \phi_0'' \rangle \sum_{t \leqslant m} \sum_{s \leqslant n} L_{mt} F_{ts} U_{sn}, \tag{9}$$

if the operator $\hat{F}$ is expanded in the intermediate basis. This is just a reexpansion in the common set of harmonic oscillator wave functions, but in contrast to an arbitrary change of basis, this expression is finite and exact. We see that when the number of quanta in at least one of the two oscillators is small, the number of elements in **L** and **U** is also small.

The procedure is easily generalized to many dimensions. Again, when only low excitations are assumed, either in the initial or final states, there is a saving. Even so, the number of states involved in the calculation can grow prohibitively large in problems with a large number of degrees of freedom. To remedy this problem at least partly, the calculation can be performed using a subspace of selected vibrational modes.

A graphical method was devised to allow easy handling of multidimensional vibration wave functions in a computer program. A graph is constructed that contains a set of vertices as seen in Fig. 1 and arcs with nonnegative slope connecting the vertices.

In the harmonic approximation, each vibration state is indexed by a string of vibration quantum numbers, $I_{vn}$

J. Chem. Phys., Vol. 112, No. 6, 8 February 2000

$^1B_{2u}$ and $^1B_{1u}$ states of benzene    2801

$=(q_1,...,q_N)$, which corresponds to a unique walk, the state path, through the graph as the one shown in Fig. 1. The slope of each arc along the path shows the number of quanta in the corresponding oscillator. Each state path has a unique ordering number that is easily and rapidly computed as the sum of certain arc weights along the path. This is analogous to the way Slater determinants can be enumerated in CI calculations.[30]

The vibrational quanta differs from electronic occupation numbers, since they can have any natural number, not only 0 or 1. This requires a modification of the conventional scheme. The weight of a vertex is defined to be, as in the electronic case, the number of paths that leads to that particular vertex.[30] However, the algebraic expression for the vertex weight is replaced by

$$W(q,K)=\sum_{i=0}^{q} W(i,K-1), \quad W(q,1)=1, \tag{10}$$

where $q$ is the number of vibration quanta in mode $K$. The paths in the subgraphs that end in vertex $(q,K)$ will be numbered from 1 to $W(q,K)$. In this implementation the strings with highest excitation in each oscillator will precede those with lower excitations, in analogy to the lexical numbering of Slater determinants in configuration interaction. The arc weight $Y(Q_{\text{from}},Q_{\text{to}},K)$ can therefore be written as

$$Y(Q_{\text{from}},Q_{\text{to}},K)=\sum_{i=Q_{\text{from}}+1}^{Q_{\text{to}}} W(i,K-1). \tag{11}$$

Each total vibration wave function has a vibration quantum number string, $I_{\text{vn}}=(q_1,...,q_N)$, which corresponds to a unique walk through the graph. Using the arc weights, each such walk has a unique ordering number, that can easily and rapidly be computed as

$$\mathcal{N}(I_{\text{vn}})=\sum_{\text{Path}} Y(Q_{\text{from}},Q_{\text{to}},K) \tag{12}$$

The recursion formulas for calculating the **L** and **U** matrices, are the time deciding step in the intensity calculation. The size of the vibrational wave function expansion for any of the electronic states grows as

$$N(Q,K)=\binom{Q+K-1}{Q}, \tag{13}$$

where $Q$ is the maximum total number of vibration quanta. If $Q_{\text{min}}=\min(Q_i,Q_f)$ and $Q_{\text{max}}=\max(Q_i,Q_f)$ and $Q_i$, $Q_f$ are the number of quanta allowed in the initial and final wave functions, respectively, then the number of floating point operations for calculating the **L** and **U** matrices is proportional to

$$K\times N(Q_{\text{max}},K)\times N(Q_{\text{min}}+1,K), \tag{14}$$

and the memory requirement will scale like $N(Q_{\text{max}},K)$ $\times N(Q_{\text{min}}+1,K)$.

## C. Transition moment derivatives

The CASSCF wave functions for the two states $\psi_1$ and $\psi_2$ are described by their CI expansions

$$\psi_1=\sum_{\mu} C_{\mu}^1 \psi_{\mu}, \tag{15}$$

$$\psi_2=\sum_{\mu} C_{\mu}^2 \psi_{\mu}, \tag{16}$$

which are built from the two orbital sets $\chi^1=(\chi_1^1\cdots\chi_N^1)$ and $\chi^2=(\chi_1^2\cdots\chi_N^2)$. The only restriction is that both states are described by the same active space and have the same spin. In order to compute transition properties the two states are transformed into a biorthogonal representation using a technique described by Malmqvist.[31] In this representation the commutator relations

$$\tilde{a}_p^\dagger a_q+a_q\tilde{a}_p^\dagger=\delta_{pq}, \tag{17}$$

$$\tilde{a}_p a_q+a_q\tilde{a}_p=0, \tag{18}$$

$$\tilde{a}_p^\dagger a_q^\dagger+a_q^\dagger\tilde{a}_p^\dagger=0, \tag{19}$$

are fulfilled, even though different basis sets are used for the two states. This is the only necessary condition for evaluating transition density matrices with standard procedures. $\tilde{a}_p^\dagger$ and $a_q^\dagger$ are the creation operators in the two biorthogonal sets. The technique has been widely used for calculating, for example, transition dipole moments.

In order to obtain derivatives of the transition properties, the wave function is expressed as a function of a perturbation strength, $\vartheta$. A unitary transformation of the reference state, $|\psi(0)\rangle$, is introduced by

$$|\psi(\vartheta)\langle=\exp(-\hat{\kappa}(\vartheta))\exp(-\hat{R}(\vartheta))|\psi(0)\rangle, \tag{20}$$

where $\hat{\kappa}$ is the antisymmetric orbital rotation operator and $\hat{R}$ the state transfer operator, which depend on the perturbation strength. Using the generators of the unitary group $\hat{E}_{ij}^-$ and state transfer operators, these antisymmetric operators can be expressed as

$$\hat{\kappa}=\sum_{p<q} \kappa_{pq}(\hat{E}_{pq}-\hat{E}_{pq})=\sum_{p<q} \kappa_{pq}\hat{E}_{pq}^-, \tag{21}$$

and

$$\hat{R}=\sum_I R_I(|\psi\rangle\langle I|-|I\rangle\langle\psi|)=\sum_I R_I\hat{P}_I. \tag{22}$$

It is important that the orbital rotation operator just contains the nonredundant rotations. This is done by excluding orbital rotations between equivalent orbitals.

A transition property $A^{12}$ can for a arbitrary perturbation strength be written as

$$A^{12}(\vartheta)=\langle\psi_1\exp(\hat{R}_1(\vartheta))\exp(\hat{\kappa}_1(\vartheta))|\hat{A}(\vartheta)|$$
$$\times\exp(-\hat{\kappa}_2(\vartheta))\exp(-\hat{R}_1(\vartheta))|\psi_2\rangle. \tag{23}$$

Having introduced a description of the transition property that is valid for all perturbation strength the derivative of the transition property can be calculated by differentiating Eq. (23).

TABLE I. Experimental and computed (Å) bond distances for the ground state of benzene.[a]

|  | $R_{CC}$ | $R_{CH}$ |
| --- | --- | --- |
| HF[a] | 1.382 | 1.072 |
| MP2[a] | 1.393 | 1.080 |
| CCSD[a] | 1.392 | 1.079 |
| CCSD(T)[b] | 1.392 | 1.081 |
| CASSCF[c] | 1.392 | 1.073 |
| CASPT2[c] | 1.396 | 1.081 |
| Exp. $R_m$[d] | 1.390 | 1.086 |
| Exp. $R_0$[e] | 1.397 | 1.085 |
| Exp. $R_0$[f] | 1.396 | 1.083 |

[a]TZ2P basis set (Ref. 35).
[b]CCSD(T) calculations, ANO $4s3p2d1f/4s2p$ basis set (Ref. 1).
[c]ANO $4s3p2d/3s2p$ basis set. Present calculations.
[d]Reference 33.
[e]Reference 49.
[f]Reference 50.

$$\frac{\partial A^{12}}{\partial \vartheta} = \langle \psi_1 | \hat{R}_1^{(\vartheta)} \hat{A} | \psi_2 \rangle - \langle \psi_1 | \hat{A} \hat{R}_2^{(\vartheta)} | \psi_2 \rangle + \langle \psi_1 | \hat{\kappa}_1^{(\vartheta)} \hat{A} | \psi_2 \rangle$$
$$- \langle \psi_1 | \hat{A} \hat{\kappa}_2^{(\vartheta)} | \psi_2 \rangle + \langle \psi_1 | \hat{A}^{(\vartheta)} | \psi_2 \rangle. \tag{24}$$

In this expression $\hat{A}^{(\vartheta)}$ is the derivative of the operator $\hat{A}$ with respect to the perturbation strength $\vartheta$. The first two terms contains only a change of the CI vectors that should be used in the evaluation of the transition density:

$$\langle \psi_1 | \hat{R}_1^{(\vartheta)} \hat{A} | \psi_2 \rangle = \sum_I R_{1I}^{(\vartheta)} \langle I | \hat{A} | \psi_2 \rangle. \tag{25}$$

To evaluate the last term, the differentiated operator is used in a standard state interaction calculation. For perturbations upon which the basis sets depend one must also describe the change of the basis set which gives the following expression for the differentiated operator:

$$\langle \psi_1 | \hat{A}^{(\vartheta)} | \psi_2 \rangle = \sum_{pq} D_{pq}^{12} \left[ A_{pq}^{(\vartheta)} + \sum_o \left[ A_{po} T_{oq}^{(\vartheta)} + T_{po}^{(\vartheta)} A_{oq} \right] \right]. \tag{26}$$

The most common choice is to use the derivative of the overlap matrix as the connection matrix ($T_{pq}$), however other choices are possible.

The product of the orbital rotation operator and the transition operator is a standard operator product between two one-particle operators and yields a two-particle operator. This in contrast to when pure expectation values are calculated, where the corresponding commutator will reduce the particle number by one. For a CASSCF wave function where the orbitals are partitioned into active (*tuvx*), inactive (*ijkl*), and secondary (*abcd*), the orbital response contribution to the transition dipole derivative will become

TABLE II. Experimental and computed (Å) bond distances for the $^1B_{2u}$ excited state of benzene.

|  | $R_{CC}$ | $R_{CH}$ |
| --- | --- | --- |
| CIS[a] | 1.414 | 1.073 |
| CCSD[b] | 1.425 | 1.078 |
| CASSCF[c] | 1.430 | 1.070 |
| CASPT2[d] | 1.432 | 1.080 |
| Expt. $R_0$[e] | 1.435 | 1.07 |
| Expt. $R_0$[f] | 1.432 | 1.084 |

[a]6-311G* basis set (Ref. 40).
[b]TZ2P basis set (Ref. 35).
[c]ANO $4s3p2d/3s2p$ basis set; six active orbitals. Present study.
[d]ANO $4s3p2d/3s2p$ basis set; 12 active orbitals. Present study.
[e]Reference 32.
[f]Reference 36.

$$\langle \psi_1 | \hat{\kappa}^\vartheta \hat{A} | \psi_2 \rangle = 2S_1^{12} \left[ \sum_{ij} \left[ A_{ii} \kappa_{jj}^\vartheta - \kappa_{ij}^\vartheta A_{ji} \right] + \sum_{pi} A_{ip} \kappa_{pi}^\vartheta \right]$$
$$+ \sum_{tu} D_{tu}^{12} \left[ \sum_i \left[ 2A_{ii} \kappa_{tu}^\vartheta + 2A_{tu} \kappa_{ii}^\vartheta \right. \right.$$
$$\left. - \kappa_{ti}^\vartheta A_{iu} - A_{ti} \kappa_{iu}^\vartheta \right] + \sum_p \kappa_{tp}^\vartheta A_{pu} \right]$$
$$+ \sum_{tuvx} d_{tuvx}^{12} A_{tu} \kappa_{vx}^\vartheta, \tag{27}$$

where $S^{12}$ is the overlap between the states and $D_{tu}^{12}$ and $d_{tuvx}^{12}$ are the transition one and two particle densities. Notice that the expectation values for the antisymmetric orbital rotation operator $\kappa^\vartheta$, even for the inactive contribution, is not necessarily equal to zero due to the fact that a biorthogonal representation is used and no symmetry restriction can be given to the representation of the orbital rotation operator.

## III. RESULTS AND DISCUSSION

### A. Geometries and energies of the ground and excited states

Tables I–III compile the experimental and theoretical bond distances for the ground and low-lying excited states of benzene. Experiments show that the ground state equilibrium structure has $D_{6h}$ symmetry.[5,32] Comparison between experimental and theoretical structures requires either that the theoretical potential is used to derive rotational constants and other spectroscopic parameters or that the experimental data are used to derive equilibrium structure and force constants. In the case of benzene, Pliva *et al.*[33] have used rotational

TABLE III. Computed (Å) bond distances for the $^1B_{1u}$ excited state of benzene.

|  | $R_{CC_1}$ | $R_{CC_2}$ | $R_{CC}(D_{6h})$ | $R_{C_1H}$ | $R_{C_2H}$ |
| --- | --- | --- | --- | --- | --- |
| CASSCF[a] | 1.437 | 1.363 | 1.411 | 1.070 | 1.070 |
| CASSCF[b] | 1.403 | 1.427 | 1.411 | 1.071 | 1.071 |
| CASPT2[c] |  |  | 1.425 | 1.081 | 1.081 |

[a]ANO $4s3p2d/3s2p$ basis set.
[b]cc-pVTZ basis set.
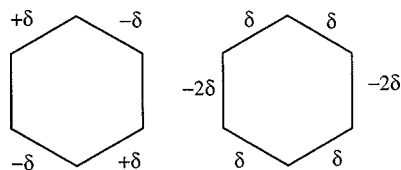[c]ANO-L ($4s3p2d/3s2p$) constrained to $D_{6h}$.

FIG. 2. The $e_{2g}$ distortions of the ring studied with an effective, fitted potential.

constants from several isotopomers to derive so-called $r_m$ bond distances. These structural parameters were devised by Watson[34] and may be regarded as a perturbation estimate to the true equilibrium structure. The perturbation parameters are the inverse square-root of the nuclear masses and a scaled inertia tensor is obtained by extrapolating to infinite masses. These bond distances are, for benzene, $r_m(CC) = 1.390(3)$ Å and $r_m(CH) = 1.086(15)$ Å. Such $r_m$ bond distances are usually very close to true $r_e$ distances, if none of the atoms is a hydrogen. On the other hand, the equilibrium structure and harmonic force field have been carefully reviewed by Martin *et al.*[1] Their recommended equilibrium distances are $r_e(CC) = 1.392(20)$ Å and $r_e(CH) = 1.081(10)$ Å, which are based on extensive CCSD(T) calculations including correction for basis set deficiency.

SCF bond lengths are usually too short because this method is unable to describe the bond breaking properly: the inherent error in the SCF method, i.e., the correlation energy, rises steeply with bond length and this effect is usually quite marked already at equilibrium geometry. A correlated treatment that includes double excitations to antibonding orbitals will allow proper dissociation. However, it is generally observed that if dynamic correlation is not included, the effects of the antibonding orbitals is often overemphasized. Therefore bond lengths computed by the CASSCF method tend to be slightly too long.

In the present CASSCF calculations, occupied $\sigma$ orbitals were inactive, while the six valence $\pi$ orbitals were active. Since this choice allows, in principle, a transformation to an equivalent set of localized orbitals, the above rules of thumb can be used. The CH bonds are not correlated and are then too short at both SCF and CASSCF levels of theory. Only the $\pi$ bonds are correlated in the CASSCF calculation, but the expected shortening due to lack of $\sigma$ correlation is not so large so we may expect the two effects to more or less cancel. In fact, as seen in Tables I and II, the CASSCF CC bond length is close to the experimental value. However, this is a fortuitous basis set effect: it is still shorter than the CCSD(T) and CASPT2 results by 0.005 Å, and Christensen *et al.*[35] has shown that the difference between the CCSD(T) result and experiment is due to basis set errors.

It has been difficult to establish conclusively the symmetry of the $1\,^1B_{2u}$ state spectroscopically.[5,32] The evidence points to $D_{6h}$ symmetry, which is obtained in all theoretical calculations.[5] Theoretical bond lengths cannot be directly compared with experiment, since only $r_0$ values are available. The theoretical $r_e$ results should fall on the low side of the experimental values. As shown by the ground state results, the CASSCF values should be reasonably accurate. The CASSCF CC distance is shorter than the CCSD value by

TABLE IV. Relative energies for the $^1B_{1u}$ state compared with the minimum $D_{2h}$ structure following the $e_{2g}$ deformation of the CC bond distances.

| Deformation ($\delta$) | Energy ($cm^{-1}$)[a] |
|---|---|
| 0.008 | 0 |
| −0.008 | 0 |
| 0.016 | 26 |
| −0.016 | 24 |
| 0.024 | 142 |
| −0.024 | 128 |
| 0.032 | 422 |
| −0.032 | 412 |
| 0 | 85 |

[a]CASSCF energies; cc-pVTZ basis set.

almost 0.005 Å and larger than the $r_0$ experimental values by about 0.005–0.002 Å.[32,36] A CASPT2 pointwise optimization was performed for the CC and CH distances with the former predicted to be 1.432 Å. The shifts in the bond distances that accompany excitation (about 0.03 Å for the CC length) are therefore very similar both in experiment and in theory. The CCSD shift is smaller than the elongation at the CASSCF and CASPT2 levels, which are very similar. This elongation has important consequences when computing the vibrational intensities. As a conclusion, although the CASSCF geometry is less accurate than the CCSD one, it is expected to lead to reasonable force fields and overlap terms for the vibrational analysis. However, as we shall see later the best agreement with experiment is obtained using the CASPT2 geometries.

The $1\,^1B_{1u}$ state is lower than, but rather close in energy to the $1\,^1E_{1u}$ state. The interaction between these two states lead to a pseudo Jahn–Teller effect which stabilizes the lower state and flattens the potential energy curve in the ring deformation modes in the $e_{2g}$ symmetry (for a description of these deformations see Fig. 2). This interaction may even lower the symmetry to $D_{2h}$. Computationally, different model errors or basis set errors will affect the amount of distortion from $D_{6h}$. Thus, at the CASSCF level, the ANO basis set and a cc-pVTZ basis set give quite different geometries. However, if analyzed in terms of vibration modes based on an averaged $D_{6h}$ structure, the difference is almost completely due to different displacements along the $e_{2g}$ coordinates, see Table IV. Electronic excitation energies are given in Table V. For the $1\,^1B_{1u}$ state both CCSD and

TABLE V. Computed and experimental excitation energies (eV).

| | CCSD[a] | CASPT2[b] | Expt.[c] |
|---|---|---|---|
| The $1\,^1B_{2u}$ state | | | |
| 0–0 | 4.93 | 4.37 | 4.72 |
| $T_e$ | 5.07 | 4.52 | ⋯ |
| Vertical | 5.22 | 4.68 | ⋯ |
| The $1\,^1B_{1u}$ state | | | |
| 0–0 | ⋯ | 5.83 | 6.03 |
| $T_e$ | ⋯ | 5.98 | ⋯ |
| Vertical | ⋯ | 6.09 | ⋯ |

[a]CCSD TZ2P; Ref. 35.
[b]ANO-L ($4s3p2d1f/3s2p1d$) one particle basis set with twelve active $\pi$-orbitals; CASPT2 geometry.
[c]Estimated from the jet-cooled spectrum; Ref. 6.

TABLE VI. Calculated and experimental harmonic frequencies ($\omega_e$, cm$^{-1}$) for the $1\ ^1A_{1g}$ ground state of benzene.

| Sym. | Modes[a] | HF[b] | MP2[b] | CCSD[b] | CC(T)[c] | CAS[d] | Obs[e] | Est[f] |
|------|------|------|------|------|------|------|------|------|
| $a_{1g}$ | $\nu_1(\nu_2)$ | 1070 | 1007 | 1015 | 1003 | 1035 | 993 | 994 |
| | $\nu_2(\nu_1)$ | 3365 | 3253 | 3245 | 3210 | 3341 | 3074 | 3191 |
| $a_{2g}$ | $\nu_3(\nu_3)$ | 1503 | 1388 | 1405 | 1380 | 1488 | 1350 | 1367 |
| $b_{2g}$ | $\nu_4(\nu_8)$ | 774 | 666 | 678 | 709 | 733 | 707 | 707 |
| | $\nu_5(\nu_7)$ | 1130 | 978 | 994 | 1009 | 1029 | 990 | 990 |
| $e_{2g}$ | $\nu_6(\nu_{18})$ | 664 | 610 | 619 | 611 | 653 | 608 | 608 |
| | $\nu_7(\nu_{15})$ | 3338 | 3226 | 3216 | 3183 | 3310 | 3057 | 3174 |
| | $\nu_8(\nu_{16})$ | 1770 | 1628 | 1656 | 1637 | 1723 | 1601 | 1608 |
| | $\nu_9(\nu_{17})$ | 1284 | 1208 | 1215 | 1194 | 1263 | 1178 | 1178 |
| $e_{1g}$ | $\nu_{10}(\nu_{11})$ | 956 | 862 | 874 | 865 | 872 | 847 | 847 |
| $a_{2u}$ | $\nu_{11}(\nu_4)$ | 759 | 688 | 696 | 687 | 710 | 674 | 674 |
| $b_{1u}$ | $\nu_{12}(\nu_6)$ | 1097 | 994 | 998 | 1020 | 1102 | 1010 | 1010 |
| | $\nu_{13}(\nu_5)$ | 3326 | 3211 | 3202 | 3173 | 3299 | 3057 | 3174 |
| $b_{2u}$ | $\nu_{14}(\nu_9)$ | 1341 | 1442 | 1302 | 1326 | 1324 | 1309 | 1309 |
| | $\nu_{15}(\nu_{10})$ | 1170 | 1186 | 1165 | 1163 | 1163 | 1150 | 1150 |
| $e_{2u}$ | $\nu_{16}(\nu_{20})$ | 450 | 406 | 411 | 406 | 433 | 398 | 398 |
| | $\nu_{17}(\nu_{19})$ | 1105 | 976 | 994 | 985 | 993 | 967 | 967 |
| $e_{1u}$ | $\nu_{18}(\nu_{14})$ | 1129 | 1058 | 1065 | 1056 | 1104 | 1038 | 1038 |
| | $\nu_{19}(\nu_{13})$ | 1636 | 1515 | 1536 | 1509 | 1615 | 1484 | 1494 |
| | $\nu_{20}(\nu_{12})$ | 3355 | 3241 | 3232 | 3200 | 3329 | 3064 | 3181 |

[a]Wilson (Ref. 26) [Herzberg (Ref. 3)] numbering of benzene modes.
[b]TZ2P basis set (Ref. 35).
[c]CCSD(T) calculations, ANO $4s3p2d1f/4s2p$ basis set (Ref. 1).
[d]ANO $4s3p2d/3s2p$ basis set. Present CASSCF calculations.
[e]Observed gas-phase fundamental frequencies. See Ref. 38.
[f]Estimated gas-phase harmonic frequencies (Ref. 38).

TABLE VII. Calculated and experimental harmonic frequencies ($\omega_e$, cm$^{-1}$) for the $1\ ^1B_{2u}$ excited state of benzene.

| Sym. | Modes[a] | CIS[b] | CCSD[c] | CAS[d] | Obs[e] |
|------|------|------|------|------|------|
| $a_{1g}$ | $\nu_1(\nu_2)$ | 922 | 955 | 958 | 923 |
| | $\nu_2(\nu_1)$ | 3054 | 3263 | 3379 | 3093 |
| $a_{2g}$ | $\nu_3(\nu_3)$ | 1333 | 1381 | 1465 | 1327 |
| $b_{2g}$ | $\nu_4(\nu_8)$ | 370 | 375 | 490 | 365 |
| | $\nu_5(\nu_7)$ | 794 | 735 | 703 | 745 |
| $e_{2g}$ | $\nu_6(\nu_{18})$ | 518 | 537 | 578 | 521 |
| | $\nu_7(\nu_{15})$ | 3026 | 3234 | 3347 | 3077 |
| | $\nu_8(\nu_{16})$ | 1556 | 1589 | 1653 | 1516 |
| | $\nu_9(\nu_{17})$ | 1140 | 1191 | 1235 | 1148 |
| $e_{1g}$ | $\nu_{10}(\nu_{11})$ | 633 | 620 | 601 | 581 |
| $a_{2u}$ | $\nu_{11}(\nu_4)$ | 575 | 558 | 532 | 515 |
| $b_{1u}$ | $\nu_{12}(\nu_6)$ | 974 | 982 | 1063 | ⋯ |
| | $\nu_{13}(\nu_5)$ | 3019 | 3224 | 3338 | ⋯ |
| $b_{2u}$ | $\nu_{14}(\nu_9)$ | 1679 | 1656 | 1821 | 1571 |
| | $\nu_{15}(\nu_{10})$ | 1145 | 1196 | 1256 | 1150 |
| $e_{2u}$ | $\nu_{16}(\nu_{20})$ | 251 | 265 | 292 | 238 |
| | $\nu_{17}(\nu_{19})$ | 771 | 757 | 675 | 717 |
| $e_{1u}$ | $\nu_{18}(\nu_{14})$ | 958 | 966 | 953 | 920 |
| | $\nu_{19}(\nu_{13})$ | 1427 | 1469 | 1537 | 1405 |
| | $\nu_{20}(\nu_{12})$ | 3042 | 3250 | 3363 | 3085 |

[a]Wilson (Ref. 26) [Herzberg (Ref. 3)] numbering of benzene modes.
[b]6-311G* basis set (Ref. 40).
[c]TZ2P basis set (Ref. 35).
[d]ANO $4s3p2d/3s2p$ basis set. Present CASSCF calculations.
[e]Observed gas-phase fundamentals (Refs. 35 and 5).

CASPT2 results are given together with the experimental 0–0 energies. Considering first the 0–0 energies we note that the CASPT2 results are lower than experiment, 0.35 and 0.20 eV for the $^1B_{2u}$ and $^1B_{1u}$ states, respectively, while the CCSD result for the $^1B_{2u}$ state is 0.22 eV too large. Christiansen and co-workers have estimated that triple corrections and additional basis set effect will lower the excitation energy to 5.80 eV in improved agreement with experiment.[35] The errors in the CASPT2 energies are somewhat larger than previously reported results for the vertical energies.[10] The reason is interesting. The computed distance between the 0–0 and vertical transitions are 0.31 and 0.26 eV for the $^1B_{2u}$ and $^1B_{1u}$ states, respectively. However for the $^1B_{2u}$ state the band maximum appear 0.19 eV above 0–0. The corresponding value for the $^1B_{1u}$ band is 0.12 eV. The vertical transitions will thus appear on the high energy side of the experimental spectrum shifted 0.12–0.14 eV from the band maximum. This shows that comparisons between band maxima and computed vertical excitation energies has to be made with some care, in particular for forbidden transitions where the intensities are not obtained from simple Franck–Condon overlap.

## B. Force fields of the ground and excited states

Tables VI, VII, and VIII list the calculated and experimental harmonic frequencies for the $1\ ^1A_{1g}$, $1\ ^1B_{2u}$, and $1\ ^1B_{1u}$ states of the benzene molecule. A description of the benzene ground state modes can be found in Refs. 26, 37, together with a careful analysis of the effects of electron correlation, basis sets, and anharmonicities[35,38,39] of the frequencies. Table VI may help to analyze the correlation effects if columns HF, MP2, and CCSD[35] are compared. An

TABLE VIII. Calculated and experimental harmonic frequencies ($\omega_e$, cm$^{-1}$) for the $1\ ^1B_{1u}$ excited state of benzene.

| Sym. | Modes[a,b] | CAS[c] | CAS[d] | CAS[e] | CAS[f] | Obs[g] | Obs[h] |
|------|------|------|------|------|------|------|------|
| $a_{1g}$ | $\nu_1(\nu_2)$ | 995 | 1021 | 1039 | 1039 | 910 | 966 |
| | $\nu_2(\nu_1)$ | 3390 | 3375 | 3338 | 3338 | ⋯ | |
| $a_{2g}$ | $\nu_3(\nu_3)$ | 1476 | | 1490 | 1490 | ⋯ | |
| $b_{2g}$ | $\nu_4(\nu_8)$ | 210 | | 568 | 568 | ⋯ | |
| | $\nu_5(\nu_7)$ | 987 | | 939 | 939 | 760 | |
| $e_{2g}$ | $\nu_6(\nu_{18})$ | 561/290 | 296 | $i$85 | 540 | 510 | |
| | $\nu_7(\nu_{15})$ | 3363/3352 | 3341 | 3306 | 3296 | ⋯ | |
| | $\nu_8(\nu_{17})$ | 1223/894 | 753 | 765 | 571 | ⋯ | 635 |
| | $\nu_9(\nu_{16})$ | 1602/1456 | 1421 | 1434 | 992 | ⋯ | |
| $e_{1g}$ | $\nu_{10}(\nu_{11})$ | 705/783 | | 773 | 773 | ⋯ | |
| $a_{2u}$ | $\nu_{11}(\nu_4)$ | 606 | | 686 | 686 | ⋯ | |
| $b_{1u}$ | $\nu_{12}(\nu_6)$ | 1120 | | 995 | 995 | ⋯ | |
| | $\nu_{13}(\nu_5)$ | 3350 | | 3295 | 3295 | ⋯ | |
| $b_{2u}$ | $\nu_{14}(\nu_9)$ | 1475 | | 1557 | 1515 | ⋯ | |
| | $\nu_{15}(\nu_{10})$ | 1258 | | 1271 | 1271 | ⋯ | |
| $e_{2u}$ | $\nu_{16}(\nu_{20})$ | 308/418 | | 311 | 311 | ⋯ | |
| | $\nu_{17}(\nu_{19})$ | 819/980 | | 920 | 920 | ⋯ | |
| $e_{1u}$ | $\nu_{18}(\nu_{14})$ | 1092/954 | 1187 | 1069 | 1069 | ⋯ | |
| | $\nu_{19}(\nu_{13})$ | 1637/1535 | 1506 | 1579 | 1579 | ⋯ | |
| | $\nu_{20}(\nu_{12})$ | 3373/3377 | 3470 | 3324 | 3324 | ⋯ | |

[a]Wilson (Ref. 26) [Herzberg (Ref. 3)] numbering of benzene modes.
[b]The label of the modes for the distorted geometries, $D_{2h}$ are identified with the corresponding modes in $D_{6h}$.
[c]ANO $4s3p2d/3s2p$ basis set. Present CASSCF calculations.
[d]cc-pVTZ basis set. Present CASSCF calculations, minima.
[e]cc-pVTZ basis set. Present CASSCF calculations, $D_{6h}$ geometry.
[f]cc-pVTZ basis set effective hessian. Present CASSCF calculations.
[g]Observed gas-phase fundamental frequencies (see Refs. 35 and 5).
[h]Observed gas-phase fundamentals. Estimated from Hiraya *et al.* (Ref. 6).

average decrease of almost 100 cm$^{-1}$ is observed from HF to CCSD values, while MP2, as usual,[35] overestimates the correlation effects on the harmonic frequencies.

The detailed CCSD(T) calculations of Martin *et al.*[1] emphasize the need of accurate basis sets as the atomic natural orbital (ANO) sets in order to obtain frequencies accurate to 10 cm$^{-1}$. The CASSCF values are, as expected, intermediate between the HF results and the results of the methods which include more correlation effects. Larger deviations in the frequencies with respect to the HF values are observed in modes with important participation of CC stretching, while the errors remain higher for modes involving especially CH bonds. In Table VII the CIS, CCSD, and CASSCF frequencies for the $1\,^1B_{2u}$ excited state can be compared. The CIS (Ref. 40) results give too low harmonic frequencies as compared both with CCSD (Ref. 35) and observed experimental values,[35,37,41–44] which are fundamental frequencies. The CCSD results[35] are probably most accurate. The largest deviation found in the CASSCF frequencies is observed in mode $\nu_{14}$, the highest frequency $b_{2u}$ mode. The poor description of the mode at the SCF level was already observed by Pulay *et al.*[45] This mode has been observed to have a strong Duschinsky mixing upon excitation. It is however more important to focus attention on the $a_{1g}$, $a_{2g}$, $e_{2u}$, and $e_{2g}$ modes, which are most important for the vibronic spectrum. The quality of the normal modes may be assessed by studying the Duschinsky rotation[14] or by computing the vibrational spectra, as will be done in the following section. For a detailed discussion of the force fields of the $1\,^1A_{1g}$ and $1\,^1B_{2u}$ states, see Ref. 35.

As discussed earlier, the $1\,^1B_{1u}$ state has a very flat energy surface in the $e_{2g}$ modes for the bond distance distortion. Distortion along this mode lowers the symmetry to $D_{2h}$. Our results show that, rather than a single $D_{6h}$ minimum, there are three equivalent $D_{2h}$ minima, very close to each other, with very small barriers between them and at the $D_{6h}$ symmetry there is a stationary point where the twofold degenerate $e_{2g}$ vibration frequency is almost zero and imaginary.

There is no point in analyzing force constants and anharmonicities at the actual equilibria. Instead, a single harmonic oscillator with $D_{6h}$ symmetry is used in the calculations. Thus the flattening is regarded as an anharmonicity, to be treated at a higher level of accuracy, also when this anharmonicity is strong enough to break the symmetry. The effective harmonic force field in the $e_{2g}$ modes was thus designed to reproduce the computed potential energies in a few points outside the flattened region. For all other modes the analytic second-order derivatives were used. This calculation was done at the CASSCF level using a cc-pVTZ basis set.

## C. Vibrational structure of the $1\,^1A_{1g} \rightarrow 1\,^1B_{2u}$ absorption band

In $D_{6h}$ symmetry, the dipole moment belongs to irrep $E_{1u}$ ($x$ and $y$ in-plane components) and $A_{2u}$ ($z$ out-of-plane component). Disregarding rotations, the ground state is totally symmetric and consists to a good approximation of the lowest vibrational state coupled to the $1\,^1A_{1g}$ electronic state. The only dipole allowed transitions at low temperature are therefore to vibronic states of $^1E_{1u}$ and $^1A_{2u}$ combined symmetry. Within the Condon approach, this will give intensity only to the $^1E_{1u}$ and $^1A_{2u}$ bands with vibrations excited primarily in totally symmetric modes due to bond length changes and maybe some weaker multiple excitations of other modes, due to different force fields and to anharmonicity. At higher order, through Herzberg–Teller coupling, transitions to other bands become possible by simultaneously exciting single quanta of nontotally symmetric modes. As an example, in the $^1B_{2u} \leftarrow \tilde{X}$ bands, the symmetry of the dipole moment matrix element is either $e_{1u}$ or $a_{2u}$ depending on the orientation of the molecule relative to the electric polarization vector. This makes the first term of the Herzberg–Teller expansion zero by symmetry and therefore the transition is forbidden. But some of the higher terms will be nonzero when the symmetry of the modes ($Q_k$, $Q_kQ_l$, etc.) combine to $b_{2u} \otimes e_{1u} \otimes a_{1g} = e_{2g}$ or $b_{2u} \otimes a_{2u} \otimes a_{1g} = b_{1g}$ There is no $b_{1g}$ vibration in benzene, so at first-order only the in-plane $e_{2g}$ modes $\nu_6$, $\nu_7$, $\nu_8$, and $\nu_9$ will induce intensity. Another way of expressing this is that the only distortions that lower the symmetry so that the $1\,^1B_{2u}$ state mixes with the one-photon allowed $1\,^1E_{1u}$ electronic state are the $e_{2g}$ vibrations. In the present set of calculations, vibrations of symmetries $e_{2g}$, $a_{1g}$, $a_{2g}$, and $e_{2u}$ have been included.

Three versions of the $^1B_{2u}$ band are shown in Fig. 3. The upper part is the experimental spectrum as recorded by Pantos *et al.* with an instrumental bandwidth of 0.8 Å (reproduced from Ref. 46). The middle band is the result of the present calculation using CASSCF force fields and the CASPT2 geometries, while the lower spectrum is based on CCSD geometries[35] and CASSCF force fields. (for structural parameters, see Tables I and II).

Since it is formally a one-photon forbidden transition, the band origin (0–0 transition) is not seen. As explained above, in order to have nonzero intensity, the transitions must involve $e_{2g}$ quanta, so the apparent or ''false'' origin is not a (0–0) but a (1–0) transition. Therefore the vibronic origins must contain quanta in modes of the $e_{2g}$ symmetry. Table IX compiles the energy, relative intensities, and assignments of the main bands showed in Fig. 3. The spectrum based on the CASPT2 geometries reproduces the available vapor spectra quite well.[32,46] Three main band systems are observed, all of them corresponding to progressions in the totally symmetric $a_{1g}\nu_1$ mode of computed frequency 958 cm$^{-1}$ (exp. 923 cm$^{-1}$, see Table VI). The two main lines are $6_0^1$ and $6_1^2$. The rest of the spectrum consists of progressions from the main lines in the totally symmetric vibrations, and $1-1, 2-2, ..., n-n$ sequences of thermally accessible vibrations, almost all of them nonsymmetrical displacements in benzene. For example, the progression of the totally symmetric mode $\nu_1$ in $6_0^1\,16_1^1$ is the second most intense in the spectrum.

The transition at 260 nm (4.8 eV) carries quanta in all of the $e_{2g}$ vibrational modes, $\nu_6$, $\nu_7$, $\nu_8$, and $\nu_9$. Any excitation of $a_{1g}$ ($\nu_1$ and $\nu_2$) and $a_{2g}$($\nu_3$) modes, combined with the $e_{2g}$ modes, give also the overall $E_{2g}$ symmetry needed for a nonzero dipole transition strength. However, since the $a_{2g}$ modes give very little intensity, they were excluded in the final calculations. Excitation of the $e_{2g}$ modes can also be
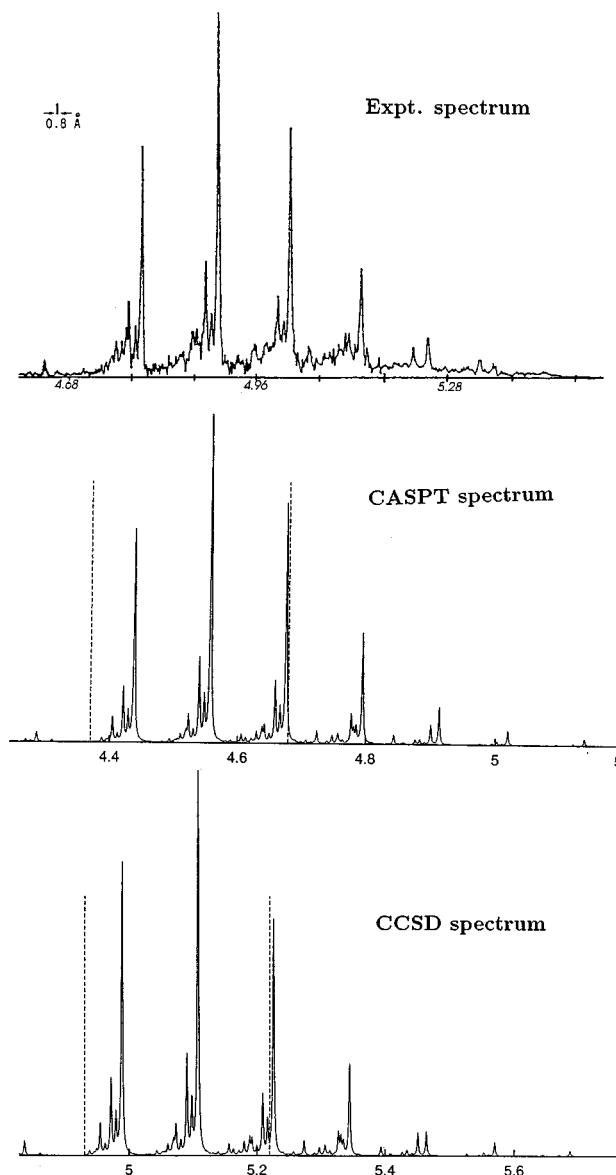
FIG. 3. The spectrum for the absorption $1\ ^1A_{1g}\rightarrow 1\ ^1B_{2u}$ in benzene. The upper spectrum is experimental (Ref. 46), the next is based on CASPT2 geometries and CASSCF force fields and transition dipole moment derivatives, and the lower spectrum is obtained using CCSD geometries. Dotted vertical lines indicate the calculated 0–0 and vertical excitation energies (Ref. 35).

TABLE IX. Computed frequencies (cm$^{-1}$) and oscillator strengths of the main vibronic bands of the $1\ ^1A_{1g}\rightarrow 1\ ^1B_{2u}$ transition in benzene.[a]

| Frequency | $f/10^{-4}$ | Assignment | Frequency | $f/10^{-4}$ | Assignment |
|---|---|---|---|---|---|
| 34 569 | 0.038 | $6_1^0$ | 37 342 | 0.037 | $6_0^1 1_1^1 16_0^2$ |
| 35 222 | 0.000 | 0-0[b] | 37 415 | 0.051 | $9_0^1 1_0^1$ |
| 35 527 | 0.058 | $6_1^0 1_0^1$ | 37 579 | 0.232 | $6_0^1 1_0^2 16_1^1$ |
| 35 663 | 0.206 | $6_0^1 16_1^1$ | 37 641 | 0.119 | $6_1^2 1_0^2$ |
| 35 725 | 0.106 | $6_1^2$ | 37 716 | 0.936 | $6_0^1 1_0^2$ |
| 35 800 | 0.831 | $6_0^1$ | 38 108 | 0.047 | $6_0^1 1_0^1 17_0^2$ |
| 36 457 | 0.033 | $9_0^1$ | 38 373 | 0.037 | $9_0^1 1_0^2$ |
| 36 484 | 0.058 | $6_0^1 1_1^1 16_2^2$ | 38 537 | 0.106 | $6_0^1 1_0^3 16_1^1$ |
| 36 485 | 0.043 | $6_0^1 1_0^2$ | 38 568 | 0.048 | $7_0^1$ |
| 36 621 | 0.317 | $6_0^1 1_1^1 16_1^1$ | 38 599 | 0.055 | $6_1^2 1_0^3$ |
| 36 683 | 0.163 | $6_1^2 1_0^1$ | 38 674 | 0.431 | $6_0^1 1_0^3$ |
| 36 758 | 1.281 | $6_0^1 1_0^1$ | 39 526 | 0.074 | $7_0^1 1_0^1$ |
| 36 875 | 0.004 | $8_0^1$ | 39 632 | 0.139 | $6_0^1 1_0^4$ |
| 37 150 | 0.031 | $6_0^1 17_0^2$ | 40 484 | 0.054 | $7_0^1 1_0^2$ |

[a]Displayed in Fig. 2. CASSCF force fields and TDM derivatives. CASPT2 excitation energy and geometries.

$e_{2u}\ \nu_{16}$ mode, with frequencies 433 and 292 cm$^{-1}$ in the ground and excited states, respectively. Excitations into this mode participate into the second strongest progression of the spectrum. Summarizing, the model includes: $e_{2g}\ \nu_6$, $\nu_7$, $\nu_8$, and $\nu_9$ modes, $a_{1g}\ \nu_1$ and $\nu_2$ modes, $a_{2g}\ \nu_3$ mode, and $e_{2u}\ \nu_{16}$ and $\nu_{17}$ modes, with excitations up to two quanta in the initial ground state and six quanta in the final excited state. The remaining modes are excluded from the calculation of the intensities, but their contribution to the overall intensity is expected to be small.

A conventional nomenclature has been introduced[32] where a mode is represented by its number and the number of quanta in the lower or upper state as a subscript or a superscript, respectively. The progression $6_0^1 1_0^n$, $n = 0, 1, 2, 3,...$ is the strongest one (Fig. 3 and Table IX) and represents excitations from the vibrationless ground state to the upper state levels with one quantum in $\nu_6$ and $n$ quanta in $\nu_1$ (0–0 transition taken from experiment). Table X compiles the experimental and computed relative intensities and oscillator strengths for the mentioned progression. Except for the jet-cooled spectrum of Stephenson *et al.*,[47] which may suffer some congestion, there is an overall agreement in obtaining the $6_0^1 1_0^1$ transition as the most intense of the spectrum, both by experiment and theory.

As pointed out above, both CASPT2 and CCSD geometries have been used in simulating the spectrum, with CASSCF force fields and TDM (transition moment derivatives) derivatives. The shift in the CC bond length in going from the ground to the excited state is 0.039, 0.033, and 0.035 Å for the CASPT2 and CCSD methods, and from experiment, respectively (see Tables I and II). It can be observed in Fig. 3 that the body of the intensity moves to higher quanta for CASPT2 geometries with respect to the spectrum computed with CCSD geometries, because of the larger change of the CC bond length at the CASPT2 level. The best agreement with the free-jet[6] and vapor-phase[32,46] spectra is obtained by using CASPT2 geometries. The match is impressive when comparison is made to the vapor-phase room temperature spectrum of Pantos *et al.*[46] (Fig. 3). Not

combined with excitation of any even number of quanta of any modes. Such double excitations of mode 16 ($e_{2u}$) lead to the second most intense progression from the $e_{2g}$ modes.

The spectrum, displayed in Fig. 3 is a combination of fundamentals, overtones, combination, and hot bands. The strongest progression carries one quanta in the $\nu_6 e_{2g}$ mode, which has been named a squashing mode due to the type of deformation caused to the ring. This is the most efficient mode for inducing intensity to the bands. The selection rule applying here is $\Delta v = \pm 1$ for the primary $e_{2g}$ coupling modes and $\Delta v = 0, \pm 1, \pm 2, \pm 3,...$ for modes $a_{1g}$ and $a_{2g}$. The remaining modes have as a selection rule $\Delta v = 0, \pm 2, \pm 4,...$ . In order to include hot bands in the computed spectrum, the most easily thermally accessible modes were included. These are the lowest frequency modes, such as the

TABLE X. Experimental and computed frequencies ($\nu$ cm$^{-1}$) absorption intensities of the $6_0^1 1_0^n$ ($n=0-4$) bands of the $^1B_{2u}\rightarrow{}^1A_{1g}$ transition in benzene. Relative values ($I$) normalized with respect to the $6_0^1$ band. Oscillator strengths ($f$) are shown within parentheses.

| | | Experimental | | | | Theoretical | |
|---|---|---|---|---|---|---|---|
| $n$ | $\nu$ [a] | $I(f/10^{-4})$ [b] | $I(f/10^{-4})$ [c] | $I$ [c] | $I$ [d] | $I(f/10^{-4})$ [e] | $I$ [f] |
| 0 | 38 611 | 1.00(1.37) | 1.00(0.88) | 1.00 | 1.00 | 1.00(1.15) | 1.00(0.83) |
| 1 | 39 533 | 1.36(1.87) | 1.72(1.51) | 1.19 | 1.38 | 1.31(1.51) | 1.54(1.28) |
| 2 | 40 458 | 0.98(0.34) | 1.48(1.31) | 0.88 | 0.90 | 0.80(0.92) | 1.13(0.94) |
| 3 | 41 377 | 0.62(0.85) | 0.77(0.68) | 0.37 | 0.37 | 0.31(0.35) | 0.52(0.43) |
| 4 | 42 297 | 0.42(0.57) | 0.40(0.35) | - | - | 0.08(0.09) | 0.16(0.14) |

[a]Frequencies in the free-jet direct absorption spectrum (Ref. 6).
[b]Integrated intensity. Jet-cooled spectrum (Ref. 6).
[c]Integrated intensity. Vapor-phase 298 and 229 K, respectively (Ref. 46).
[d]Computed integrated intensity (Ref. 51).
[e]Present computed integrated intensity. CCSD geometries, CASSCF force fields, and TDM derivatives.
[f]Present computed integrated intensity, CASPT2 geometries, CASSCF force fields, and TDM derivatives.

surprisingly, the relative intensities of the vibrational progressions constitute a sensitive measure of the exactness of computed relative geometries.

Table XI lists experimental and theoretical relative intensities for the $e_{2g}$ vibronic origins of this band of benzene taken from the calculation using the CCSD geometries. The $6_0^1$ origin is by far which carries most of the intensity of the spectrum. Our computed intensities for the $e_{2g}$ origins, independently of the geometry used for the states, match quite nicely the observed jet-cooled and vapor-phase band intensities. Previous theoretical calculations at the CIS/6-31+G* level[14] seemed to overestimate the intensity associated to the $8_0^1$ origin.

As a summary, the computed spectrum for the $1\,^1A_{1g}\rightarrow 1\,^1B_{2u}$ transition of benzene using CASSCF force fields successfully reproduced the main features observed in the experimental spectra and improves previous theoretical results. The results obtained here do not pretend to be used for a fine analysis of such a well-known and studied spectrum, but as a benchmark for the method and level of the calculations. No scaling has been included in the model and the CASSCF harmonic frequencies are not extremely accurate. The obtained force field seems however to be of reasonable quality for the vibronic analysis of the spectrum. The best agreement with experiment is obtained when the geometry shift between the states is as accurate as possible. Obviously,

TABLE XI. Experimental and computed frequencies (cm$^{-1}$) and absorption intensities of the vibronically induced $e_{2g}$ false origins for the $^1B_{2u}\rightarrow{}^1A_{1g}$ transition in benzene. Relative values ($I$) normalized with respect to $6_0^1$.

| | Experimental | | | Theoretical | |
|---|---|---|---|---|---|
| Trans. | $\nu$ [a] | $\epsilon$ [a] | $I$ [b] | CIS [c] | CAS [d] |
| $6_0^1$ | 38 606 | 100.0 | 100.0 | 100.0 | 100.0 |
| $7_0^1$ | 41 159 | 3.6 | 5.9 | 3.0 | 5.8 |
| $8_0^1$ | 39 602 | 0.6 | ⋯ | 5.8 | 0.4 |
| $9_0^1$ | 39 233 | 1.8 | 2.3 | 0.3 | 4.0 |

[a]Jet-cooled spectrum (Ref. 47). Normalized peak heights.
[b]Vapor room-temperature spectrum (Ref. 32). Integrated intensity.
[c]Relative intensities computed at the CIS/6-31+G* level (Ref. 14).
[d]Present computed integrated intensity, CASPT2 geometries, CASSCF force fields, and TDM derivatives.

further effects can be included in the model such as second-order Herzberg–Teller couplings (the second-order allowed transition $1_0^1 17_0^2$ is clearly observed in the experimental spectrum)[47] or the inclusion of the degeneracy terms.

## D. Vibrational structure of the $1\,^1A_{1g}\rightarrow 1\,^1B_{1u}$ absorption band

The $^1B_{1u}$ state is more complicated to treat than the $^1B_{2u}$ state. First of all the energy surface is flat and distorted, which makes an anharmonic treatment necessary for an accurate quantitative analysis. This can, in principle, be done by the LU approach, since all types of matrix elements can be computed with this approach. However, the present code employs a polynomial approximation for the potential and transition moments and it is easily seen that a polynomial that represents correctly the threefold symmetry of these functions will have at least degree 6. Furthermore, truncated polynomials are not suitable for this purpose. In this study we have instead replaced the potential by an effective harmonic potential and kept the $D_{6h}$ symmetry. The harmonic potential was chosen to approximate the true potential for larger displacements in the $e_{2g}$ modes. The pseudo Jahn–Teller effect will cause large anharmonic deviations from the computed spectrum. We expect that the excitation energies will be too high, as compared to a correct anharmonic calculation, but that the qualitative features will come out correctly. Nonadiabatic coupling is also expected to be of importance to this state, but it has not been included in the present study.

For the $^1B_{2u}\leftarrow\widetilde{X}$ band, the $z$ (out of plane) component of the field did not contribute to any intensity. This is not the case for $^1B_{1u}\leftarrow\widetilde{X}$, where all components of the field may contribute to the spectrum. Transitions in this band require the simultaneous excitation (or deexcitation) of vibrational quanta with a combined symmetry of either $b_{1u}\otimes e_{1u}\otimes a_{1g} = e_{2g}$ or $b_{1u}\otimes a_{2u}\otimes a_{1g} = b_{2g}$. Consequently, $e_{2g}$ and $b_{2g}$ modes have to be included. Also, bond length changes induce progressions with excited modes and the hot bands require inclusion of the low frequencies $e_{2u}$ vibrations. Thus, vibrations of symmetries $e_{2g}$, $a_{1g}$, $b_{2g}$, and $e_{2u}$ were included in the calculations.
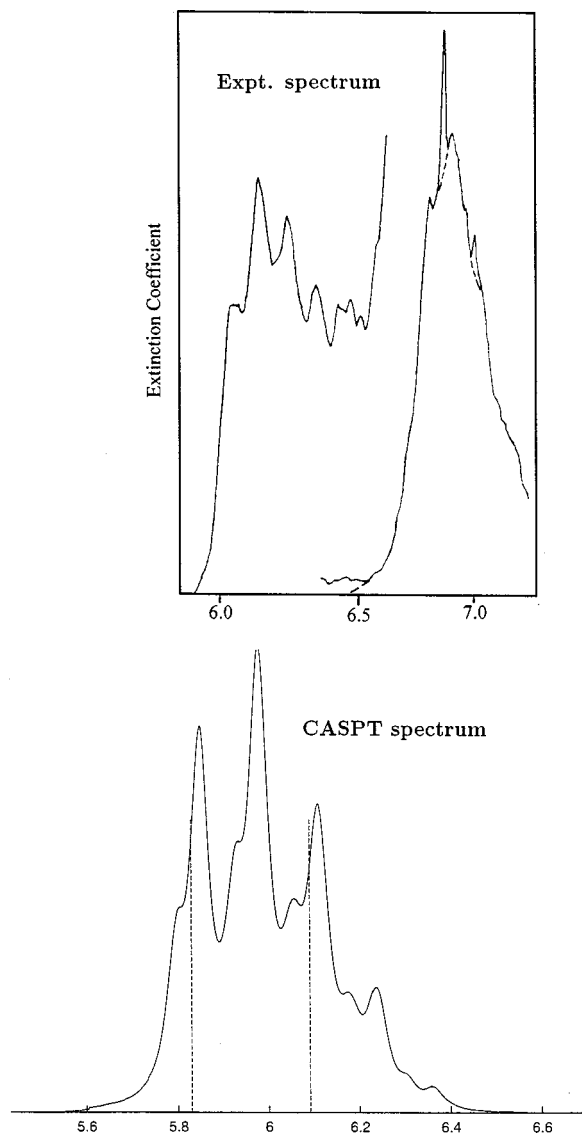
FIG. 4. The spectrum for the absorption 1 $^1A_{1g} \rightarrow 1\ ^1B_{1u}$ in benzene. Upper curve is the experimental spectrum (Ref. 46), lower curve the computed spectrum based on CASPT2 geometries and CASSCF force fields, and transition dipole moment derivatives. Dotted vertical lines indicate the calculated 0–0 and vertical excitation energies.

TABLE XII. Computed frequencies (cm$^{-1}$) and oscillator strengths of the main vibronic bands of the 1 $^1A_{1g} \rightarrow 1\ ^1B_{1u}$ transition in benzene.

| Frequency | $f/10^{-4}$ | Assignment | Frequency | $f/10^{-4}$ | Assignment |
|---|---|---|---|---|---|
| 46 214 | 0.00 | 0–0 | 48 833 | 5.8 | $1_0^2 6_0^1$ |
| 46 785 | 43.0 | $8_0^1$ | 48 876 | 1.5 | $1_0^1 6_0^3$ |
| 46 755 | 11.7 | $6_0^1$ | 48 876 | 0.0 | $6_0^5$ |
| 47 088 | 35.9 | $9_0^1 16_1^1$ | 49 073 | 2.1 | $4_0^5$ |
| 47 173 | 3.8 | $5_0^1$ | 49 167 | 17.8 | $1_0^2 9_0^1 16_1^1$ |
| 47 206 | 144.9 | $9_0^1$ | 49 190 | 9.5 | $9_0^3$ |
| 47 825 | 42.8 | $1_0^1 8_0^1$ | 49 285 | 71.8 | $1_0^2 9_0^1$ |
| 47 794 | 11.6 | $1_0^1 6_0^1$ | 49 389 | 19.8 | $1_0^1 8_0^2 9_0^1$ |
| 47 828 | 3.1 | $9_0^1 16_0^2$ | 49 327 | 10.3 | $1_0^1 6_0^2 9_0^1$ |
| 47 929 | 6.7 | $8_0^3$ | 49 370 | 0.7 | $6_0^4 9_0^1$ |
| 47 898 | 2.7 | $6_0^1 8_0^2$ | 49 903 | 7.1 | $1_0^3 8_0^1$ |
| 47 836 | 1.5 | $6_0^3$ | 49 873 | 1.9 | $1_0^3 6_0^1$ |
| 47 836 | 0.0 | $1_0^1 9_0^1 4_0^1$ | 49 873 | 0.0 | $6_0^3 9_0^2$ |
| 48 128 | 35.7 | $1_0^1 9_0^1 16_1^1$ | 49 915 | 0.8 | $1_0^2 6_0^3$ |
| 48 213 | 3.8 | $1_0^1 5_0^1$ | 50 206 | 5.9 | $1_0^3 9_0^1 16_1^1$ |
| 48 245 | 144.1 | $1_0^1 9_0^1$ | 50 324 | 23.9 | $1_0^3 9_0^1$ |
| 48 349 | 19.9 | $8_0^2 9_0^1$ | 50 428 | 9.8 | $1_0^2 8_0^2 9_0^1$ |
| 48 319 | 6.8 | $6_0^1 8_0^1 9_0^1$ | 50 366 | 5.1 | $1_0^2 6_0^2 9_0^1$ |
| 48 288 | 10.3 | $6_0^2 9_0^1$ | 50 366 | 0.0 | $6_0^1 9_0^4$ |
| 48 739 | 1.4 | $9_0^2 6_0^1$ | 51 363 | 6.0 | $1_0^4 9_0^1$ |
| 48 864 | 21.4 | $1_0^2 8_0^1$ | | | |

field for the $^1B_{1u}$ state. It is very sensitive to the details of the interaction between the $^1B_{1u}$ and $^1E_{1u}$ states. An accurate treatment of the adiabatic spectrum will also aid the study of nonadiabatic effects.

As in the $^1B_{2u}$ case, the strongest lines in the vibronic spectra in the $^1B_{1u}$ band consist of a progression in the $\nu_1$ $a_{1g}$ mode built on the $e_{2g}$ modes. The main peak corresponds to the $9_0^1 1_0^n$ progression, where the in-plane mode $\nu_9$ has a frequency of 992 cm$^{-1}$. The second strongest progression is built on the other $e_{2g}$ mode, $\nu_6$, with a frequency of 540 cm$^{-1}$. The weaker peaks corresponds to combinations of the other $e_{2g}$ modes and the symmetric modes plus hot bands especially in the $\nu_{16}$ $e_{2u}$ mode.

The selection rules for the transition from the $^1A_{1g}$ to $^1B_{1u}$ state is the same as for the $^1B_{2u}$ transition, due to the fact that no symmetry distortion or higher-order terms than a harmonic approximation has been included. The present results favor the previous interpretation of the spectrum based on matrix spectra of benzene.[4,48] The close presence of other transition to states such as the Rydberg $3s$ or the most intense $^1E_{1u}$ valence state makes the analysis of the experimental spectra a difficult task.

Figure 4 and Table XII show the computed 1 $^1B_{1u} \leftarrow 1\ ^1A_{1g}$ absorption band, using CASPT2 geometries, harmonic CASSCF force fields, and transition dipole moment (TDM) derivatives. The experimental spectrum is also shown in the figure.[46] To see the resemblance between the calculated and experimental spectra, the lines in the computed spectrum have been broadened, corresponding to a lifetime of 8 fs. The hot bands at room temperature are included in the plot. As already mentioned, instead of a correct anharmonic treatment of the $^1B_{1u}$ state, an effective harmonic potential was chosen. In spite of this, the theoretical spectrum reproduces the main features of the experimental spectrum reasonably well even if the relative intensities do not show the same match as they did for the $^1B_{2u}$ state. This is most certainly due to the uncertainty of the change of geometry due to the flatness and anharmonicity of the upper surface. Work is in progress to describe the anharmonic force

## IV. CONCLUSIONS

The two lowest bands of the electronic spectrum of the benzene molecule have been studied theoretically using a new method to compute vibronic excitation energies and intensities. A harmonic force field has been assumed for the ground state, the $^1B_{2u}$ and the $^1B_{1u}$ electronic states. A linear approximation has been used for the transition dipole as a function of the nuclear displacement coordinates. A LU partitioning technique was used to compute the matrix elements of the vibrational wave functions for the two electronic

states. The derivative of the transition dipole was computed using a variant of the CASSCF state interaction method, CASSI.

Force fields and transition dipole elements were computed using CASSCF wave functions with six active $\pi$-orbitals. Absolute excitation energies were obtained from more accurate CASPT2 calculations using an active space of 12 $\pi$-orbitals. Comparison was also made using results obtained in a recent CCSD study of the ${}^1B_{2u}$ state.[35]

The results show that the model works well. The vibrational progressions are well described in both bands and in excellent agreement with experiment. Computed intensities are also in good agreement with experiment, in particular when CASPT2 derived geometries are used. One interesting result is that computed vertical energies fall about 0.1 eV on the high energy side of the band maximum. Future work within this project will include the effects of anharmonicities and nonadiabatic couplings between different electronic states.

## ACKNOWLEDGMENTS

[1] J. M. L. Martin, P. R. Taylor, and T. J. Lee, Chem. Phys. Lett. **275**, 414 (1997).

[2] *Quantum Mechanical Electronic Structure Calculations with Chemical Accuracy*, edited by S. R. Langhoff (Kluwer, Dordrecht, The Netherlands, 1995).

[3] G. Herzberg, *Molecular Spectra and Molecular Structure. III. Electronic Spectra and Electronic Structure of Polyatomic Molecules* (Van Nostrand, New York, 1966).

[4] M. B. Robin, *Higher Excited States of Polyatomic Molecules* (Academic, New York, 1975), Vol. II.

[5] B. S. Hudson and L. D. Ziegler, in *The Vibronic Spectroscopy of Benzene: Old Problems and New Techniques*, Excited States, edited by E. C. Lim (Academic Press, New York, 1982), Vol. 5.

[6] A. Hiraya and K. Shobatake, J. Chem. Phys. **94**, 7700 (1991).

[7] P. G. Wilkinson, Can. J. Phys. **34**, 596 (1956).

[8] N. Nakashima, M. Sumitani, I. Ohmine, and K. Yoshihara, J. Chem. Phys. **72**, 2226 (1980).

[9] B. O. Roos, K. Andersson, and M. P. Fülscher, Chem. Phys. Lett. **192**, 5 (1992).

[10] J. Lorentzon, P.-Å Malmqvist, M. P. Fülscher, and B. O. Roos, Theor. Chim. Acta **91**, 91 (1995).

[11] M. J. Packer, E. K. Dalskov, T. Enevoldsen, and H. J. Aa. Jensen, J. Chem. Phys. **105**, 5886 (1996).

[12] O. Christiansen, H. Koch, A. Halkier, and P. Jørgensen, J. Chem. Phys. **105**, 6921 (1996).

[13] J. E. Del Bene, J. D. Watts, and R. J. Bartlett, J. Chem. Phys. **106**, 6051 (1997).

[14] G. Orlandi, P. Palmieri, R. Tarroni, F. Zerbetto, and M. Z. Zgierski, J. Chem. Phys. **100**, 2458 (1994).

[15] H. Köppel, W. Domcke, and L. S. Cederbaum, Adv. Chem. Phys. **57**, 59 (1984).

[16] A. M. Mebel, M. Hayasi, and S. H. Lin, Chem. Phys. Lett. **274**, 281 (1997).

[17] Y. Luo, H. Ågren, S. Knuts, B. F. Minaev, and P. Jørgensen, Chem. Phys. Lett. **209**, 513 (1993).

[18] B. O. Roos, in *The Complete Active Space Self-Consistent Field Method and its Applications in Electronic Structure Calculations*, Advances in Chemical Physics; *Ab Initio* Methods in Quantum Chemistry, edited by K. P. Lawley (Wiley, Chichester, England, 1987), Vol. II, Chap. 69, p. 339.

[19] A. Bernhardsson, R. Lindh, M. P. Fülscher, and J. Olsen, Mol. Phys. **96**, 617 (1999).

[20] P. Å. Malmqvist and B. O. Roos, Chem. Phys. Lett. **155**, 189 (1989).

[21] P.-O. Widmark, P.-Å. Malmqvist, and B. O. Roos, Theor. Chim. Acta **77**, 291 (1990).

[22] K. Andersson, P.-Å. Malmqvist, B. O. Roos, A. J. Sadlej, and K. Wolinski, J. Phys. Chem. **94**, 5483 (1990).

[23] K. Andersson, P.-Å. Malmqvist, and B. O. Roos, J. Chem. Phys. **96**, 1218 (1992).

[24] B. O. Roos, K. Andersson, M. P. Fülscher, P.-Å. Malmqvist, L. Serrano-Andrés, K. Pierloot, and M. Merchán, in *Multiconfigurational Perturbation Theory: Applications in Electronic Spectroscopy*, in Advances in Chemical Physics: New Methods in Computational Quantum Mechanics, edited by I. Prigogine and S. A. Rice (Wiley, New York, 1996), Vol. XCIII:219.

[25] S. Califano, *Vibrational States* (Wiley, London, 1976).

[26] E. B. Wilson, J. C. Decius, and P. C. Cross, *Molecular Vibrations* (McGraw-Hill, New York, 1955).

[27] G. Fischer, *Vibronic Coupling. The Interaction Between the Electronic and Nuclear Motion* (Academic, London, 1984).

[28] P.-Å. Malmqvist and N. Forsberg, Chem. Phys. **228**, 227 (1998).

[29] MOLCAS Version 4.0, K. Andersson, M. R. A. Blomberg, M. P. Fülscher, G. Karlström, R. Lindh, P.-Å. Malmqvist, P. Neogrády, J. Olsen, B. O. Roos, A. J. Sadlej, M. Schütz, L. Seijo, L. Serrano-Andrés, P. E. M. Siegbahn, and P.-O. Widmark, Dept. of Theor. Chem., Chem. Center, Univ. of Lund, P.O.B. 124, S-221 00 Lund, Sweden, Lund, 1997.

[30] W. Duch, *GRMS or Graphical Representation of Model Spaces* (Springer-Verlag, Berlin, 1986).

[31] P.-Å. Malmqvist, Int. J. Quantum Chem. **30**, 479 (1986).

[32] J. H. Callomon, T. M. Dunn, and I. M. Mills, Philos. Trans. R. Soc. London, Ser. A **259**, 499 (1966).

[33] J. Pliva, J. W. C. Johns, and L. Goodman, J. Mol. Spectrosc. **148**, 427 (1991).

[34] J. K. G. Watson, J. Mol. Spectrosc. **48**, 479 (1973).

[35] O. Christiansen, J. F. Stanton, and J. Gauss, J. Chem. Phys. **108**, 3987 (1998).

[36] J. R. Lombardi, R. Wallenstein, T. W. Hänsch, and D. M. Friedrich, J. Chem. Phys. **65**, 2357 (1976).

[37] R. H. Page, Y. R. Shen, and Y. T. Lee, J. Chem. Phys. **88**, 5362 (1988).

[38] L. Goodman, A. G. Ozkabak, and S. N. Thakur, J. Phys. Chem. **95**, 9044 (1991).

[39] P. E. Maslen, N. C. Handy, R. D. Amos, and D. Jayatilaka, J. Chem. Phys. **97**, 4233 (1992).

[40] G. S. Jas and K. Kuczera, Chem. Phys. **214**, 229 (1997).

[41] G. H. Atkinson and C. S. Parmenter, J. Mol. Spectrosc. **73**, 31 (1978).

[42] G. H. Atkinson and C. S. Parmenter, J. Mol. Spectrosc. **73**, 20 (1978).

[43] G. H. Atkinson and C. S. Parmenter, J. Mol. Spectrosc. **73**, 52 (1978).

[44] N. Mikami and M. Ito, J. Chem. Phys. **64**, 3077 (1976).

[45] P. Pulay, G. Fogarasi, and J. E. Boggs, J. Chem. Phys. **74**, 3999 (1981).

[46] E. Pantos, J. Philis, and A. Bolorinos, J. Mol. Spectrosc. **72**, 36 (1978).

[47] T. A. Stephenson, P. L. Radloff, and S. A. Rice, J. Chem. Phys. **81**, 1060 (1984).

[48] B. Katz, M. Brith, A. Ron, B. Sharf, and J. Jortner, Chem. Phys. Lett. **2**, 189 (1968).

[49] B. P. Stoicheff, Can. J. Phys. **20**, 65 (1952).

[50] A. Cabana, J. Bachand, and J. Giguere, Can. J. Phys. **52**, 1949 (1974).

[51] G. Fischer, S. Jakobson, and R. Naaman, Chem. Phys. Lett. **49**, 427 (1977).